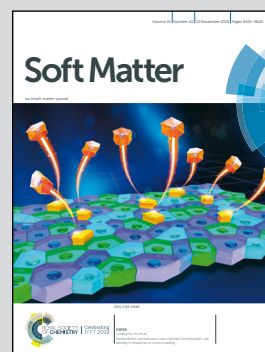


Highlighting research from the Smart Materials and Structures Laboratory from the group of Chaofeng Lü

Prescribing patterns in growing tubular soft matter by initial residual stress

We designed experiments on growing soft tubes to demonstrate the strong impact of initial residual stress on the creation of wrinkle patterns. Here we prescribed the initial stress to create a 3D pattern on the inner face of a hydrogel tube, showing an interaction between axial and circumferential wrinkles. We then modelled the phenomenon mathematically.

As featured in:



See Chaofeng Lü *et al.*,
Soft Matter, 2019, 15, 8468.



Cite this: *Soft Matter*, 2019,
15, 8468

Prescribing patterns in growing tubular soft matter by initial residual stress

Yangkun Du,^{id ab} Chaofeng Lü,^{id *cde} Congshan Liu,^c Zilong Han,^a Jian Li,^a
Weiqiu Chen,^{ade} Shaoxing Qu,^{id ade} and Michel Destrade^{id ab}

Initial residual stress is omnipresent in biological tissues and soft matter, and can affect growth-induced pattern selection significantly. Here we demonstrate this effect experimentally by letting soft tubes grow in the presence or absence of initial residual stress and by observing different growth pattern evolutions. These experiments motivate us to model the mechanisms at play when a growing bilayer tubular organ spontaneously displays buckling patterns on its inner surface. We demonstrate that not only differential growth, geometry and elasticity, but also initial residual stress distribution, exert a notable influence on these pattern phenomena. Prescribing an initial residual stress distribution offers an alternative or a more effective way to implement pattern selection for growable bio-tissues or soft matter. The results also show promise for the design of 4D bio-mimic printing protocols or for controlling hydrogel actuators.

Received 3rd August 2019,
Accepted 18th September 2019

DOI: 10.1039/c9sm01563a

rsc.li/soft-matter-journal

1 Introduction

Pattern creation in soft matter is a ubiquitous phenomenon in Nature and is now being promoted in biomedical and industrial applications. In biological systems, specific patterns are used to maintain essential bio-functions such as the wrinkles found in the intestine (Fig. 1A), useful for digesting, and the interconnected creases of the brain cortex, associated with intelligence development.^{1,2} Other patterns are used to transmit pathological changes: hence, an abnormally wrinkled airway is a marker for asthmatic bronchiole, and frequent morphological changes of a tumour point to a pre-metastatic state.³ In other words, Nature and Evolution have mastered well how to control and select optimal patterns for soft tissues. In turn, engineers try to mimic these processes to create and control ideal patterns in manufacturing. For example, self-assembly of a substrate–film structure for 3D micro-fabrication is achieved by local mismatch deformation between substrate and film: the resulting substrate curvature underpins spontaneous micro- or nano-patterns and structures.^{4–6} Similarly, stimuli-responsive hydrogel actuators can be designed by prescribing inhomogeneous swelling and made to wrinkle into different patterns.

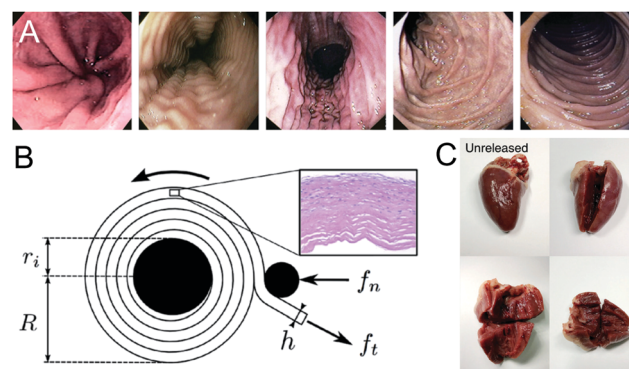


Fig. 1 (A) Different morphological wrinkling patterns along the human intestine;⁷ (B) a protocol for printing non-Euclidean solids, similar to 3D-printing bio-tissues in bioengineering;⁸ (C) residual stresses can be released in a duck heart by cutting it in different directions.⁹

Physically, wrinkle/crease patterns are created by mechanically-induced instability and post-buckling processes. The striking case of spontaneous instability and post-buckling in the absence of external loads can be explained by the presence of inhomogeneous residual stress fields. These stresses have been revealed experimentally in many bio-tissues such as skin, arteries, heart, brain, intestine, solid tumors, *etc.*,^{1,10–15} where they are required to ensure self-equilibrium, transfer bio-signals, or maintain some specific bio-functions.^{16–18} They can also endow elastic materials with prescribed properties (Fig. 1B).

A strong and sustained research effort has been dedicated to the modelling of growth-induced residual stresses and the resulting pattern-generating instabilities.^{1,19–22} These papers used volume growth theory,²³ where growth is initiated from

^a Department of Engineering Mechanics, Zhejiang University, Hangzhou, P. R. China

^b School of Mathematics, Statistics and Applied Mathematics, NUI Galway, Galway, Ireland

^c Department of Civil Engineering, Zhejiang University, Hangzhou 310058, P. R. China. E-mail: lucf@zju.edu.cn; Fax: +86-571-8820-8685; Tel: +86-571-8820-8473

^d Key Lab of Soft Machines and Smart Devices of Zhejiang Province, Zhejiang University, Hangzhou, P. R. China

^e Soft Matter Research Center, Zhejiang University, Hangzhou 310027, P. R. China

an initially stress-free configuration. In particular, the influence of differential volume growth and growth velocity on the creation of residual stress in bilayer cylinders was elucidated, resulting in a pattern selection protocol which can be tuned by changing thickness and stiffness ratios.^{1,2,3–25}

However, most living tissues do not possess a stress-free initial configuration, as can be checked by cutting them in different directions: each additional cut releases more residual stress and consequently an infinite number of cuts would be required in principle to attain this hypothetical zero stress initial configuration (see the examples of a cut duck heart in Fig. 1C or cut human arteries in ref. 10). In reality, long-term growth and remodelling processes and other complex bio-interactions are impossible to track and reconstruct for living matter. Hence, the stress-free assumption for the initial state is too strong for real biological soft matter, and neglecting initial residual stress may affect the analysis of growth-induced residual stress and the resulting pattern selection.

In a previous paper,²⁶ we used an experimentally-determined initial residual stress distribution to explain theoretically how a human aorta could experience different stress distributions and eventually buckle with growth. For the present paper, we design a simple yet effective experimental setup to reveal in a controlled, robust and reproducible way the influence of initial residual stress on growth and pattern buckling for a bilayer tube. Then for our modelling, we take a linear distribution of the initial radial stress through the thickness of the tube (instead of the specific and complex experimental distribution in the aorta²⁶). With this simple model, we are able to uncover qualitatively all possible pattern formations in the tube, also in agreement with our experimental results. Both our experimental and theoretical results give the consistent conclusion that initial residual stress affects the growth-induced residual stress and the resulting pattern evolution, and also do a significant impact on the onset of critical buckling, a threshold which is very important to determine in practice.

We structure the paper as follows. In Section 2, we describe our experimental setup and track (with photographs) the evolution of the resulting pattern phenomena. We see that they give a measure of the influence of initial residual stresses on growth and morphogenesis. Section 3 provides mathematical modelling of the experiments, based on growth and instability analyses. In Sections 4 and 5, we present and discuss the results.

2 Experiments

We designed experiments on tubular bilayer structures, made of a hydrogel tube inside a rubber tube, and placed in water where the hydrogel swells. One bilayer tube is initially stress-free, the other is subject to an initial stress achieved by shrink-fit.

2.1 Protocol

First, we prescribed an initial residual stress by setting an incompatible geometry for the two separate parts (hydrogel and rubber). Hence we set the outer face of the inner hydrogel

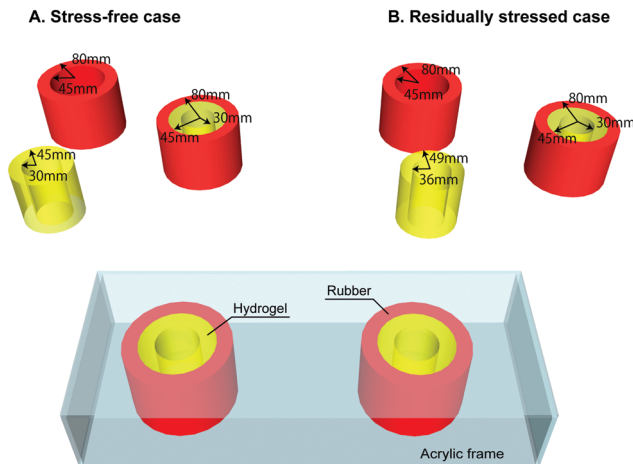


Fig. 2 Experimental setup for isotropic growth-induced instability of two bilayer tubes, one with non-zero initial residual stress, one without.

tube to have a slightly larger radius than the radius of the inner face of the outer rubber tube. Then we expanded the external rubber tube and forced the hydrogel tube into it, thus creating a compressive hoop stress in the hydrogel and a tensile hoop stress in the rubber. We measured the changes in radii due to the shrink-fitting and found them to be negligible (less than 3%).

For direct comparison with the case where there is no initial stress, we nested another hydrogel tube into another rubber tube, with the same geometry and materials as in the first bilayer tube, but without any geometrical mismatch (the outer radius of the hydrogel tube was equal to the inner radius of the rubber tube).

All tubes were 7 cm tall. The inner radius of the bilayer tubes was $R_i = 30$ mm, the radius at the interface was $R_s \approx 45$ mm, and the outer radius was $R_o = 80$ mm, giving radii ratios $R_o/R_s \approx 1.8$, $R_s/R_i = 1.5$. The elastic modulus of the hydrogel and the rubber are 87 kPa and 448 kPa, respectively, giving a stiffness ratio $\mu^{\text{inn}}/\mu^{\text{out}} \approx 0.2$.

We then placed the two bilayer tubes in an Acrylic frame, with fixed top and bottom plates, to prevent axial stretch, see the experimental setup shown in Fig. 2. We pierced two circular holes on both the top and bottom plates, with centres on the axis of the tubes, for water to flow freely during the growth period.

Finally, the frame and tubes were placed in a big water tank.

2.2 Materials

Hydrogel: *N,N*-methylenebis(acrylamide) 98% (MBAA, Lot #146072) and ammonium persulfate 98% (APS, Lot #248614) were purchased from Sigma-Aldrich (St. Louis, Missouri, United States); Acrylamide 99% (AAM, Lot #A108465) was purchased from Aladdin (Shanghai, China). All reagents were used as received.

Rubber: VytaFlex™ 30 was purchased from Smooth-On (Macungie, United States).

2.3 Preparation

Hydrogel: first, the AAM monomer was dissolved in distilled water to form a solution of concentration 4 mol L⁻¹. Then, to

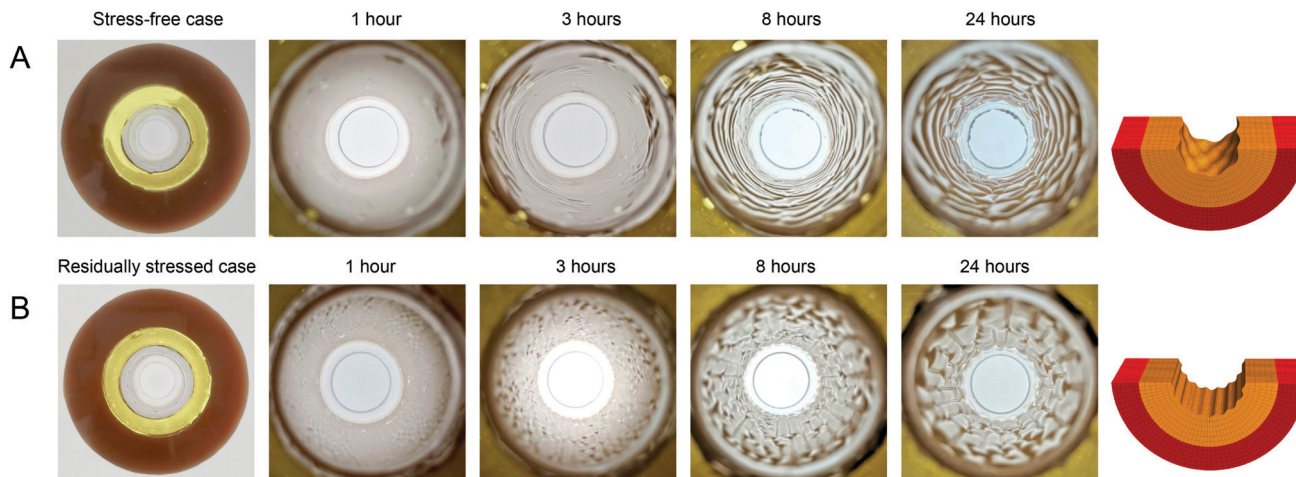


Fig. 3 Growth-induced buckling of bilayer tubes (inner layer: swelling hydrogel, outer layer: inert rubber) with (A) stress-free and (B) residually stressed initial states. By shrink-fitting, we created a non-zero initial residual stress in (B) (compressive hoop stress in the hydrogel, tensile hoop stress in the rubber). Otherwise, (A) and (B) have the same initial geometry and material parameters ($R_o/R_s \approx 1.8$, $R_s/R_i = 1.5$, $\mu^{inn}/\mu^{out} \approx 0.2$). Axial growth is prevented. Once submerged in water, (B) buckles earlier and in a different pattern (wrinkle-front aligned with the axis) than (A) (mixed axial/circumferential wrinkles).

every 1 ml of the solution, 4 μl of a 0.1 mol L^{-1} of MBAA solution were added as the conventional cross-linker, and 20 μl of a 0.1 mol L^{-1} ammonium persulfate solution were added as the ultra-violet (UV) initiator. The resulting solution was degassed by N_2 for 1 hour and then poured into a mould made of laser-cut acrylic sheets. The mould and the solution were covered with the bottom of a Petri dish to prevent oxygen inhibition. The covered mould was then placed under a UV lamp and exposed to UV irradiation (wavelength = 365 nm). Finally, the resulting hydrogel tube was taken out of the mould, washed with de-ionised water thoroughly to remove any unreacted monomers, and was kept at room temperature.

Rubber: see the fabrication instructions at <http://www.smooth-on.com.cn/uploadfile/2018/0510/20180510040704891.pdf>.

2.4 Experimental results

Fig. 3 provides experimental proof of the impact of initial residual stress on growth-induced pattern creation and evolution.

The two bilayer tubes had the same geometry, were made from the same materials, but were under different initial residual stresses prior to growth. The prescribed initial residual stresses were: stress-free for one bilayer tube (Fig. 3A), and compressive hoop stress in hydrogel and tensile hoop stress in rubber for the other (Fig. 3B).

The results show that by imposing an initial residual stress, we can bring forward the onset of instability and also create a pattern with straight circumferential folds along the axial direction, as opposed to the postponed, mixed circumferential and axial folds shown in Fig. 3A.

3 Modelling

3.1 Growth with initial residual stress

Here we show that the so-called ‘modified multiplicative decomposition growth’ (MMDG) model^{9,26} is consistent with our experimental findings.

The MMDG framework relies on the concept of multiplicative decomposition,²⁷ similar to the conventional volumetric growth model.²³ Its innovation lies in the introduction of an initial elastic deformation \mathbf{F}_0 which is used for releasing the initial residual stress to a virtual stress-free configuration. Thereafter, the independent unconstrained growth process \mathbf{F}_g can take place freely, using two virtual stress-free and incompatible configurations. The elastic deformation \mathbf{F}_e then makes the material compatible again. Accordingly, the total growth process can be formulated by the deformation gradient

$$\mathbf{F} = \mathbf{F}_e \mathbf{F}_g \mathbf{F}_0. \quad (1)$$

Here, we assume that the material in its virtual stress-free state is an incompressible neo-Hookean solid. Its strain energy function is

$$\psi = \frac{\mu}{2} [\text{tr}(\mathbf{F}_e^T \mathbf{F}_e) - 3], \quad (2)$$

where μ is the initial shear modulus. Also, with the relationship $\mathbf{F}_g \mathbf{F}_g^T = \frac{\boldsymbol{\tau} + p_0 \mathbf{I}}{\mu}$, the constitutive equation²⁶ for isotropic growth is

$$\boldsymbol{\sigma} = J_g^{-\frac{2}{3}} (\mathbf{F} \boldsymbol{\tau} \mathbf{F}^T + p_0 \mathbf{F} \mathbf{F}^T) - p \mathbf{I}, \quad (3)$$

where p , p_0 are the Lagrange multipliers in current and reference configurations, respectively, and $J_g = \det \mathbf{F}_g$ tracks local volume change. The initial stress $\boldsymbol{\tau}$ and the Cauchy stress $\boldsymbol{\sigma}$ satisfy the equilibrium equations and boundary conditions in each configuration,

$$\text{Div } \boldsymbol{\tau} = 0, \quad \boldsymbol{\tau}^T \mathbf{N} = 0, \quad \text{div } \boldsymbol{\sigma} = 0, \quad \boldsymbol{\sigma}^T \mathbf{n} = 0 \quad (4)$$

where \mathbf{n} , \mathbf{N} are unit vectors normal to the boundary.

3.2 Geometry and initial residual stress field

For comparison with known results on pattern selection in growing tubular soft solids,²⁸ we characterise our bilayer tube as being typical of bio-tissues. Hence, we take shear moduli in the ranges $\mu^{\text{inn}} = 120\text{--}700$ Pa, $\mu^{\text{out}} = 1$ kPa (close to those of embryonic gastrointestinal tissue). We take the outer layer radius $R_o = 1$, interface radius $R_s = R_o/1.8$ and inner radius R_i as a geometric variable.

To reproduce the initial residual stress in the experiments and in some bilayer tissues, we approximate the variations of the radial initial residual stress with R to be linear, close to the calculated distribution resulting from shrink-fit.²⁹ Hence we take

$$\tau_{RR}^{\text{inn}} = \alpha \frac{R - R_i}{R_i - R_s}, \quad \tau_{RR}^{\text{out}} = \alpha \frac{R - R_o}{R_o - R_s}, \quad (5)$$

which satisfy the required boundary conditions at the inner (R_i), interface (R_s) and outer (R_o) surfaces of the bilayer. We take the axial initial residual stress as $\tau_{ZZ}^{\text{inn}} = \tau_{ZZ}^{\text{out}} = 0$. Then we obtain the distribution of the circumferential stress $\tau_{\theta\theta}$ by solving $\text{Div } \tau = 0$, the self-equilibrium equation for the initial residual stress.

The initial residual stress field in eqn (5) is compressive radial stress τ_{RR} and leads to a hoop stress $\tau_{\theta\theta}$ which is compressive (tensile) in the inner (outer) layer, reproducing the qualitative characteristics of our experiments on hydrogel/rubber tubes. We pre-multiply this initial residual stress distribution by a magnitude factor α , which we use to quantify the influence of the initial stress: $\alpha = 0$ means a totally stress-free initial state, $\alpha > 0$ means the inner layer is under compressive hoop initial stress (as in our experiments), $\alpha < 0$ means the outer layer is hoop-compressed initially. Finally we call g^{inn} , g^{out} the volumetric growth factors in the inner and outer layers, respectively, and we solve the corresponding buckling boundary value problem.

3.3 Buckling analysis

The onset of instability is analysed by relying on incremental theory³⁰ and on our previous papers.^{9,26}

In short, there exists a relation giving the increment \dot{F} of the displacement gradient F with respect to the reference configuration as $\dot{F} = \dot{F}_1 F$, where \dot{F}_1 is the incremental displacement gradient with respect to the current configuration. Since the growth process is assumed to be independent of the stress and strain fields due to the infinitesimal and transient incremental deformation, we also have the relationship $\dot{F}_e = \dot{F}_1 F_e$ for the pure elastic gradient F_e and its increment.

By prescribing the incremental displacement field as

$$\dot{\mathbf{x}} = u(r, \theta, z) \mathbf{e}_r + v(r, \theta, z) \mathbf{e}_\theta + w(r, \theta, z) \mathbf{e}_z, \quad (6)$$

we get the incremental displacement gradient tensor as

$$\dot{F}_1 = \frac{\partial \dot{\mathbf{x}}}{\partial \mathbf{x}} = \begin{bmatrix} \frac{\partial u}{\partial r} & \frac{1}{r} \left(\frac{\partial u}{\partial \theta} - v \right) & \frac{\partial u}{\partial z} \\ \frac{\partial v}{\partial r} & \frac{1}{r} \left(\frac{\partial v}{\partial \theta} + u \right) & \frac{\partial v}{\partial z} \\ \frac{\partial w}{\partial r} & \frac{1}{r} \frac{\partial w}{\partial \theta} & \frac{\partial w}{\partial z} \end{bmatrix}. \quad (7)$$

Then the incremental incompressibility condition reads

$$\text{tr } \dot{F}_1 = \frac{\partial u}{\partial r} + \frac{1}{r} \left(\frac{\partial v}{\partial \theta} + u \right) + \frac{\partial w}{\partial z} = 0. \quad (8)$$

Now the incremental nominal stress \dot{S} in push-forward form has components

$$\dot{S}_{ij} = \mathcal{A}_{ijkl}^1 \dot{F}_{1lk} - \dot{p} \delta_{ij} + p \dot{F}_{1ij}, \quad (9)$$

where $\mathcal{A}_{cijkl}^1 = F_{ciz} F_{ck\beta} \frac{\partial \psi}{\partial F_{ej\alpha} \partial F_{cl\beta}}$ are the components of the instantaneous elasticity tensor, calculated by differentiating the strain energy density Ψ leading to the constitutive relation eqn (3). Finally, the incremental equilibrium equations and boundary conditions are:

$$\text{div } \dot{S}_1 = 0, \quad \dot{S}_1^T \mathbf{n} = 0. \quad (10)$$

The shapes of the incremental displacement fields are specified as m circumferential and n axial sinusoidal wrinkles, in the form $[u, v] = [U(r), Q(r)] \cos(m\theta) \cos(\kappa z)$, $v = V(r) \sin(m\theta) \cos(\kappa z)$, $w = W(r) \sin(m\theta) \cos(\kappa z)$, where m and $\kappa = 2\pi n/L$ are the circumferential and axial wave-numbers, respectively. Then the incremental nominal stress components are of similar forms: $\dot{S}_{1rr} = \Sigma_{rr}(r) \cos(m\theta) \cos(\kappa z)$, $\dot{S}_{1r\theta} = \Sigma_{r\theta}(r) \sin(m\theta) \cos(\kappa z)$, $\dot{S}_{1rz} = \Sigma_{rz}(r) \cos(m\theta) \sin(\kappa z)$. Eventually we arrive at the Stroh formulation of the incremental equations of equilibrium, see ref. 9 and 26 for details and components of the Stroh matrix $G(r)$,

$$\frac{d}{dr} \boldsymbol{\eta}(r) = \frac{1}{r} G(r) \boldsymbol{\eta}(r), \quad (11)$$

where

$$\boldsymbol{\eta}(r) = [U(r), V(r), W(r), r \Sigma_{rr}(r), r \Sigma_{r\theta}(r), r \Sigma_{rz}(r)]^T, \quad (12)$$

is the displacement-traction Stroh vector.

Finally, by iterating over the wrinkle numbers m and n for the numerical solution of eqn (12), we obtain the critical value of each case which creates a buckling pattern for some given differential growth ratio. Here, we use the surface impedance method for a robust numerical integration of the incremental equations.^{31–34}

4 Results

The numerical strategy is to find the smallest differential growth ratio $g^{\text{inn}}/g^{\text{out}}$ for which an incremental solution exists, for given wrinkle numbers n , m . Then after spanning all possible wrinkle numbers in the circumferential and axial directions, we keep the smallest ratio $(g^{\text{inn}}/g^{\text{out}})_{\text{cr}}$ for the onset of buckling. If the corresponding n_{cr} , m_{cr} are both non-zero, then the wrinkling pattern is two-dimensional.

According to the expression of the initial residual stress in eqn (5), we can recover instability results with a stress-free initial state by prescribing $\alpha = 0$, and use the results as benchmark results, see Fig. 4. Hence we see that increasing the thickness or stiffness ratio of the outer to inner tubes will create fewer folds in the circumferential direction and more folds in the axial direction. An in-depth analysis of pattern

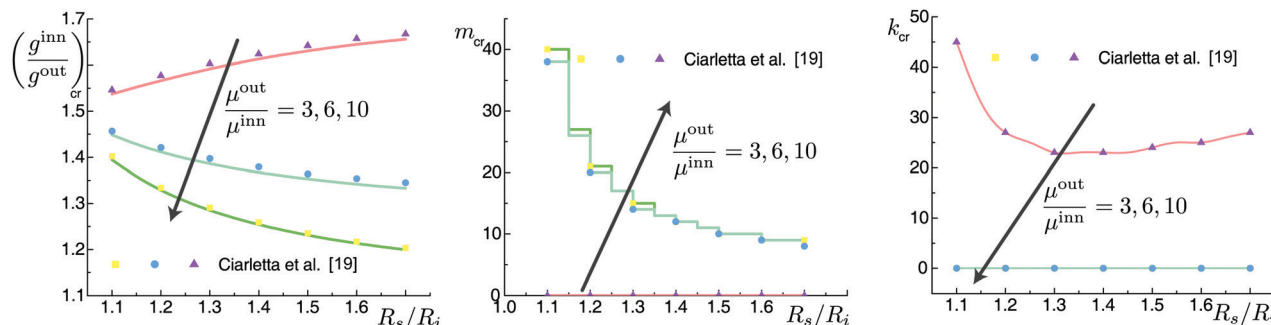


Fig. 4 Benchmark results of growth-induced instability without initial residual stress,²⁸ where $R_o/R_s = 1.8$, $R_o = 1$, $g^{ad} = 1$.

selection by these factors has been conducted by Ciarletta *et al.*²⁸

In that case, which is not realistic for actual living matter (Fig. 1B), pattern selection can only be tuned by the geometric and elastic parameters. Starting then from an initially stressed state $\alpha \neq 0$, we find that pattern selection can be largely tuned or prescribed by the magnitude α of the initial stress τ .

Generally, soft tubular tissues are too soft to sustain increasing levels of initial residual stresses for long, especially compressive hoop stresses, which quickly induce buckling patterns in the absence of growth (when $(g^{in}/g^{ad})_{cr} = 1$) and external loads.³⁵ Here we find that this occurs when the amplitude of the initial stress is large enough. Hence, wrinkles appear on the inner face of the composite tube when $\alpha > \alpha_{upp} \simeq 1.003$, and on its outer face when $\alpha < \alpha_{low} \simeq -4.560$ (as the outer layer is then under large compressive hoop stress), see Fig. 5.

Otherwise, when $\alpha_{low} < \alpha < \alpha_{upp}$, instability is due to combined high levels of initial stress and differential growth. Fig. 5 and 6 show the effect of the initial stress magnitude α on the evolution of growth-induced patterns. Fig. 5 shows that with initial residual stress ($\alpha \neq 0$), the level of differential growth $(g^{inn}/g^{out})_{cr}$ required for buckling is reduced. It is worth noting here that this calculation result is consistent with our experimental finding in Fig. 3 that the stress-free case occurs wrinkles earlier than the residual stress case.

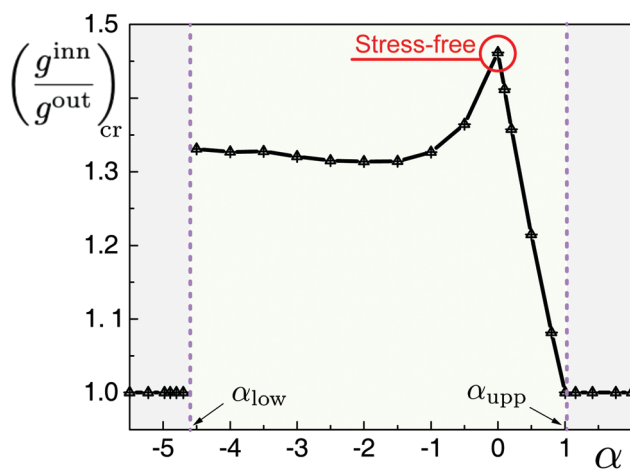


Fig. 5 Variation of the critical differential growth ratio $(g^{inn}/g^{out})_{cr}$ with the level of initial stress α , when the stiffness ratio is $\mu^{inn}/\mu^{out} = 1/5$.

Fig. 6 gives the numbers of circumferential and axial wrinkles. In the pure growth-induced case ($\alpha = 0$), a 2D-pattern is predicted ($m_{cr} = 7$, $n_{cr} = 2$), consistent with our experiments (Fig. 3A), where the buckling mode is a mix of circumferential and axial wrinkles. Then, increasing the initial circumferential compressive stress in the inner layer with $\alpha > 0$ increases m_{cr} and decreases n_{cr} . Quickly (see zoom of the $-0.1 < \alpha < 0.1$ range in Fig. 6B), $n_{cr} = 0$ and the wrinkles are aligned with the tube axis, again consistent with our experiments (Fig. 3B), showing that compressive initial residual stress facilitates the circumferential wrinkles. Conversely, reversing the location of circumferential compressive and tensile stresses by taking $\alpha < 0$ leads to $m_{cr} = 0$. Fig. 6B further displays the details and profiles of possible patterns around $\alpha = 0$, and shows how sensitive they are to initial residual stress.

Effectively, the gamut of the wrinkling scenarios encountered in the intestine (Fig. 1A) can be captured by varying the magnitude and the sign of α only, while keeping the geometric and material parameters the same throughout. The figures demonstrate how to obtain, control and advance pattern creation by prescribing initial residual stress fields for given elasticities and geometries.

5 Conclusions

We investigated the natural capability of biological epithelial tissues to use initial residual stresses to control pattern creation, based on a recently developed growth model, and we also mimicked the results experimentally by swelling hydrogel tubes.

We then showed that initial stress is an effective and controllable factor for pattern selection beyond the geometric and elastic parameters highlighted in previous studies of pure growth.²⁸ We also showed that there is an effective range $\alpha_{low} < \alpha < \alpha_{upp}$ for the level of initial stress where patterns can be prescribed on growable bio-tissues.

We did not expand the instability analysis beyond the linearised buckling state, but it is worth noting that wrinkles are very stable for layered structures and give the number and wavelength of the eventual super-critical creases.³⁶ They are also a way to measure the level of a known distribution of initial stress.³⁵

Our hope is that these results may provide an inspiring insight for directional bionic self-assembly or robot manufacturing by initial residual stress.

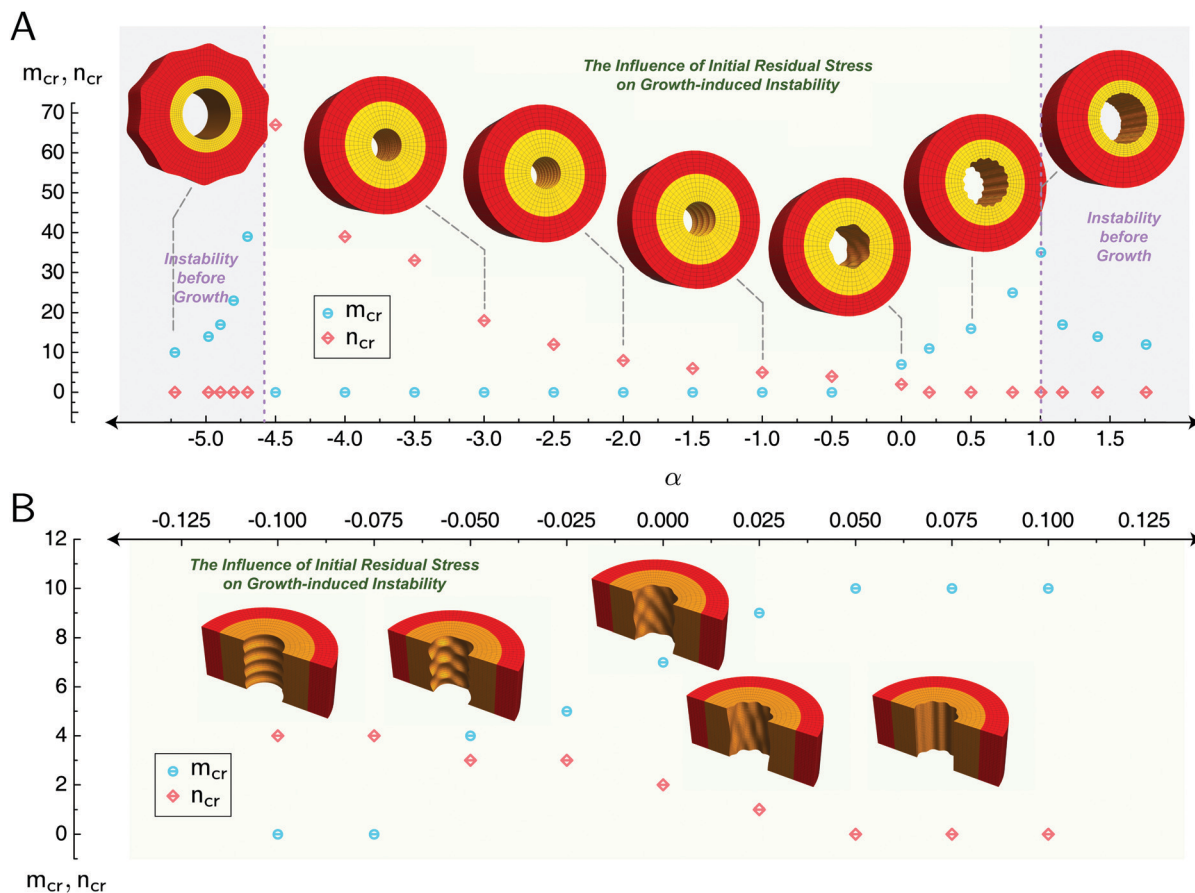


Fig. 6 (A) Effect of the magnitude of the initial residual stresses α on growth-induced pattern selection, when $\mu^{inn}/\mu^{out} = 1/5$; (B) zoom of the results in the range $-0.01 < \alpha < 0.01$ in (A).

Conflicts of interest

There are no conflicts to declare.

Acknowledgements

We gratefully acknowledge support from National Natural Science Foundation of China (grants 11621062/11772295) and China Scholarship Council.

References

- V. Balbi, E. Kuhl and P. Ciarletta, *J. Mech. Phys. Solids*, 2015, **78**, 493–510.
- J. Altman and S. A. Bayer, *The human brain during the second trimester*, CRC Press, 2005.
- E. T. Roussos, J. S. Condeelis and A. Patsialou, *Nat. Rev. Cancer*, 2011, **11**, 573 EP.
- J. Yin, E. Bar-Kochba and X. Chen, *Soft Matter*, 2009, **5**, 3469–3474.
- X. Chen and J. Yin, *Soft Matter*, 2010, **6**, 5667–5680.
- X. Chen, *Mechanical Self-Assembly: Science and Applications*, Springer Science & Business Media, 2012.
- C. M. Wilcox, M. Muñoz-Navas and J. J. Sung, *Atlas of Clinical Gastrointestinal Endoscopy E-Book: Expert Consult-Online and Print*, Elsevier Health Sciences, 2012.
- G. Zurlo and L. Truskinovsky, *Phys. Rev. Lett.*, 2017, **119**, 048001.
- Y. Du, C. Lü, W. Chen and M. Destrade, *J. Mech. Phys. Solids*, 2018, **118**, 133–151.
- G. A. Holzapfel, G. Sommer, M. Auer, P. Regitnig and R. W. Ogden, *Ann. Biomed. Eng.*, 2007, **35**, 530–545.
- G. A. Holzapfel and R. W. Ogden, *J. R. Soc., Interface*, 2010, **7**, 787–799.
- J. H. Omens and Y.-C. Fung, *Circ. Res.*, 1990, **66**, 37–45.
- T. Savin, N. A. Kurpios, A. E. Shyer, P. Florescu, H. Liang, L. Mahadevan and C. J. Tabin, *Nature*, 2011, **476**, 57–62.
- T. Stylianopoulos, J. D. Martin, V. P. Chauhan, S. R. Jain, B. Diop-Frimpong, N. Bardeesy, B. L. Smith, C. R. Ferrone, F. J. Hornicek, Y. Boucher, L. L. Munn and R. K. Jain, *Proc. Natl. Acad. Sci. U. S. A.*, 2012, **109**, 15101–15108.
- M. E. Fernandez-Sanchez, S. Barbier, J. Whitehead, G. Bealle, A. Michel, H. Latorre-Ossa, C. Rey, L. Fouassier, A. Claperon, L. Brulle, E. Girard, N. Servant, T. Rio-Frio, H. Marie, S. Lesieur, C. Housset, J. L. Gennisson, M. Tanter, C. Menager, S. Fre, S. Robine and E. Farge, *Nature*, 2015, **523**, 92–95.

- 16 Y. Pan, I. Heemskerk, C. Ibar, B. I. Shraiman and K. D. Irvine, *Proc. Natl. Acad. Sci. U. S. A.*, 2016, 201615012.
- 17 T. P. Padera, B. R. Stoll, J. B. Tooredman, D. Capen, E. D. Tomaso and R. K. Jain, *Nature*, 2004, **427**, 695.
- 18 G. Helmlinger, P. A. Netti, H. C. Lichtenbeld, R. J. Melder and R. K. Jain, *Nat. Biotechnol.*, 1997, **15**, 778.
- 19 Y.-P. Cao, B. Li and X.-Q. Feng, *Soft Matter*, 2012, **8**, 556–562.
- 20 B. Li, Y.-P. Cao, X.-Q. Feng and H. Gao, *J. Mech. Phys. Solids*, 2011, **59**, 758–774.
- 21 C. Lü and Y. Du, *Int. J. Appl. Mech.*, 2016, **8**, 1640010.
- 22 Y. Du and C. Lü, *Theor. Appl. Mech. Lett.*, 2017, **7**, 117–120.
- 23 E. K. Rodriguez, A. Hoger and A. D. McCulloch, *J. Biomech.*, 1994, **27**, 455–467.
- 24 A. Goriely and M. Ben Amar, *Phys. Rev. Lett.*, 2005, **94**, 198103.
- 25 P. Ciarletta, *Phys. Rev. Lett.*, 2013, **110**, 158102.
- 26 Y. Du, C. Lü, W. Chen and M. Destrade, *Sci. Rep.*, 2019, **9**, 8232.
- 27 S. Sadik and A. Yavari, *Math. Mech. Solids*, 2015, **22**, 771–772.
- 28 P. Ciarletta, V. Balbi and E. Kuhl, *Phys. Rev. Lett.*, 2014, **113**, 248101.
- 29 P. Pedersen, *Comput. Mech.*, 2006, **37**, 121–130.
- 30 R. W. Ogden, *Non-linear elastic deformations*, Courier Corporation, 1997.
- 31 S. Biryukov, *Sov. Phys. Acoust.*, 1985, **31**, 350–354.
- 32 M. Destrade, J. Murphy and R. Ogden, *Int. J. Eng. Sci.*, 2010, **48**, 1212–1224.
- 33 M. Destrade, A. N. Annaidh and C. D. Coman, *Int. J. Solids Struct.*, 2009, **46**, 4322–4330.
- 34 Y. Su, B. Wu, W. Chen and M. Destrade, *J. Mech. Phys. Solids*, 2019, DOI: 10.1016/j.jmps.2019.07.013.
- 35 P. Ciarletta, M. Destrade, A. L. Gower and M. Taffetani, *J. Mech. Phys. Solids*, 2016, **90**, 242–253.
- 36 Y. Cao and J. W. Hutchinson, *Proc. R. Soc., Ser. A*, 2011, **468**, 94–115.